PLOS ONE

RESEARCH ARTICLE

Time Dependent MHD Nano-Second Grade Fluid Flow Induced by Permeable Vertical Sheet with Mixed Convection and Thermal Radiation

Muhammad Ramzan[1]*, **Muhammad Bilal**[2]

1 Department of Mathematics, College of Science, Majmaah University, Al-Zulfi, Saudi Arabia, **2** Department of Mathematics, Faculty of Computing, Mohammad Ali Jinnah University, Islamabad Campus, Islamabad, Pakistan

* m.ramzan@mu.edu.sa

Citation: Ramzan M, Bilal M (2015) Time Dependent MHD Nano-Second Grade Fluid Flow Induced by Permeable Vertical Sheet with Mixed Convection and Thermal Radiation. PLoS ONE 10(5): e0124929. doi:10.1371/journal.pone.0124929

Academic Editor: Zhonghao Rao, China University of Mining and Technology, CHINA

Received: January 10, 2015

Accepted: March 6, 2015

Published: May 11, 2015

Data Availability Statement: The authors confirm that all data underlying the findings are fully available without restriction. All relevant data are within the paper.

Funding: This project is funded by the Deanship of Scientific Research (DSR), Majmaah University, Saudi Arabia under project no. 36-1-5. The author, therefore, acknowledges with thanks DSR for its financial support. The funders had no role in study design, data collection and analysis, decision to publish, or preparation of the manuscript.

Abstract

The aim of present paper is to study the series solution of time dependent MHD second grade incompressible nanofluid towards a stretching sheet. The effects of mixed convection and thermal radiation are also taken into account. Because of nanofluid model, effects Brownian motion and thermophoresis are encountered. The resulting nonlinear momentum, heat and concentration equations are simplified using appropriate transformations. Series solutions have been obtained for velocity, temperature and nanoparticle fraction profiles using Homotopy Analysis Method (HAM). Convergence of the acquired solution is discussed critically. Behavior of velocity, temperature and concentration profiles on the prominent parameters is depicted and argued graphically. It is observed that temperature and concentration profiles show similar behavior for thermophoresis parameter *Nt* but opposite tendency is noted in case of Brownian motion parameter *Nb*. It is further analyzed that suction parameter *S* and Hartman number *M* depict decreasing behavior on velocity profile.

Introduction

Many engineering and industrial applications involve a working fluid that may be active or inactive in its own capacity. The role of this fluid is to transfer energy/heat from one location to other. For a long period, the performance of adequate heat transfer has been a major problem. The introduction of nanofluid as a working fluid has opened the gates of new era in the area of heat transfer. With thermal conductivity more than base fluid and a size of 1–100 nm, nanoparticles are utilized to attain the maximum enhancement in the thermal characteristics under minimum concentrations. The pioneering work of Choi [1] with the declaration that thermal conductivity of base fluid will be doubled by adding the nanoparticles into the base fluid revolutionized the related engineering applications in a variety of directions. These include coolants of nuclear reactors, cancer therapy, safer surgeries and in safety problems related to nuclear

Competing Interests: The authors have declared that no competing interests exist.

reactors. In designing the waste heat removal equipment, nanoparticles play an important role [2]. With both liquid and magnetic properties, magneto nanofluid with its varied biomedical applications like sterilized devices, wound treatment, gastric medications, asthma treatment and elimination of tumors has a vital role in daily life. Some recent studies on nanofluids and magneto nanofluids may be found in the references [3–12] and many therein.

Comprehensive knowledge of non-Newtonian fluids' flow characteristics is the need of the day because of their vital role in growing industrial and engineering applications. These may include shampoos, soaps, apple sauce, polymeric liquids, tomato paste, ketchup, paints, blood at low shear rate etc. The Navier-Stokes equations are not sufficient to explore the true behavior of such materials. Different types of non-Newtonian fluid models are developed in the past to describe the actual behavior of these liquids. The fluid model which is used in the present investigation is a subclass of differential type non-Newtonian fluids and known as second grade fluid. This fluid model is capable to explore the shear thinning and shear thickening effects. Fetecau et al. [13] studied the unsteady flow of second grade fluid induced due to the time-dependent motion of wall. They provided the exact solutions of this flow analysis by employing Fourier sine transform. Helical flows of second grade fluid between two coaxial cylinders are investigated by Jamil et al. [14]. Here the flow generation is due to inner cylinder motion. Hayat et al. [15] reported two dimensional boundary layer flow of second grade fluid with convective boundary condition via homotopy analysis method. Turkyilmazoglu [16] discussed the dual and triple solutions of MHD second grade non-Newtonian fluid in the presence of slip condition. Heat transfer analysis in viscoelastic non-Newtonian fluid flow is discussed by Ashorynejad et al. [17]. Heat source effect in second grade fluid in the presence of power law heat flux condition is explored by Hayat et al. [18]. Hayat et. al [19] discussed the stratifications and mixed convection radiative flow of Jeffrey fluid over a stretching sheet. But very less approaches have been reported in the presence of nanofluids.

To bridge this gap, we have studied the thermal radiation effects in MHD unsteady flow of second grade nanofluid in the presence of mixed convection. The flow is induced due to the vertical stretching sheet. We developed series solutions of velocity, temperature and nanoparticle concentration via homotopy analysis method (HAM) [20–26]. Graphs are plotted to examine the effects of various physical parameters on the dimensionless temperature and nanoparticle concentration fields. Values of skin-friction coefficient, local Nusselt and Sherwood numbers are computed and discussed. From the literature survey, it is revealed that no such analysis is reported yet.

Mathematical formulation

We consider the magnetohydrodynamics (MHD) and time dependent flow of an incompressible second grade nanofluid over a porous stretching surface. The electrically conducting fluid under the influence of a unsteady magnetic field $B(t)$ which is applied in a direction normal to the stretching surface. Under the assumption of a small magnetic Reynolds number, the induced magnetic field is negligible. Moreover, heat transfer process is also taken into account. The geometrical configuration of the present flow is shown in Fig 1.

The governing boundary layer equations using above mentioned suppositions and Boussineq's approximation can be written as:

$$\frac{\partial u}{\partial x}+\frac{\partial v}{\partial y}=0, \tag{1}$$

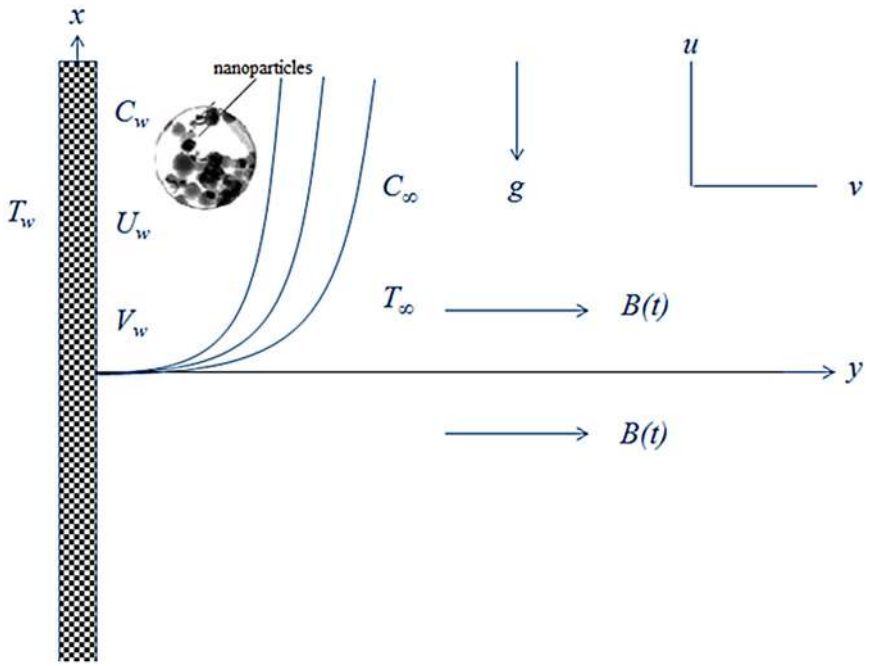

Fig 1. Geometry of the problem.

doi:10.1371/journal.pone.0124929.g001

$$\frac{\partial u}{\partial t}+u\frac{\partial u}{\partial x}+v\frac{\partial u}{\partial y} = v\frac{\partial^2 u}{\partial y^2}+\frac{\alpha_1}{\rho}\left(\frac{\partial^3 u}{\partial t\partial y^2}+u\frac{\partial^3 u}{\partial x\partial y^2}+\frac{\partial u}{\partial x}\frac{\partial^2 u}{\partial y^2}+\frac{\partial u}{\partial y}\frac{\partial^2 v}{\partial y^2}+v\frac{\partial^3 u}{\partial y^3}\right)+ g\beta_T(T-T_\infty)+g\beta_C(C-C_\infty)-\frac{\sigma B^2(t)u}{\rho}, \tag{2}$$

$$\rho C_P\left(\frac{\partial T}{\partial t}+u\frac{\partial T}{\partial x}+v\frac{\partial T}{\partial y}\right) = \alpha_1\left(\frac{\partial^2 u}{\partial y\partial t}\frac{\partial u}{\partial y}+u\frac{\partial^2 u}{\partial x\partial y}\frac{\partial u}{\partial y}+v\frac{\partial^2 u}{\partial y^2}\frac{\partial u}{\partial y}\right)+k\frac{\partial^2 T}{\partial y^2}+ \mu\left(\frac{\partial u}{\partial y}\right)^2-\frac{\partial q_r}{\partial y}+\tau\left(D_B\frac{\partial C}{\partial y}\frac{\partial T}{\partial y}+\frac{D_T}{T_\infty}\left(\frac{\partial T}{\partial y}\right)^2\right), \tag{3}$$

$$\frac{\partial C}{\partial t}+u\frac{\partial C}{\partial x}+v\frac{\partial C}{\partial y}=D_B\frac{\partial^2 C}{\partial y^2}+\frac{D_T}{T_\infty}\frac{\partial^2 T}{\partial y^2}. \tag{4}$$

By using Rosseland approximatoin for radiation we have

$$q_r=-\frac{4\sigma^*}{3k^*}\frac{\partial T^4}{\partial y}, \tag{5}$$

in which q_r the radiative heat flux in the y-direction, g the gravitational acceleration, T the fluid temperature, σ^* the Stefan-Boltzmann constant, v the kinematic viscosity, σ the electrical conductivity, ρ the fluid density, β_C and β_T are the concentration and thermal expansion coefficients respectively, D_B and D_T are the Brownian diffusion coefficient and thermophoretic diffusion coefficient, respectively, k^* is the mean absorption coefficient, α_1 the second grade

parameter and C_p the specific heat and. Since the fluid abide by the second law of thermodynamics and the assumption that the specific Helmholtz free energy is least when the fluid is at a constant temperature then we have $\mu \geq 0, \alpha_1 \geq 0, \alpha_1 + \alpha_2 = 0$.

Expanding T^4 in Taylor series about T_∞ and neglecting higher terms, we found

$$T^4 \cong 4T_\infty^3 T - 3T_\infty^4 \tag{6}$$

By making use of Eqs (5) and (6), Eq (3) has the following form

$$\begin{aligned} \rho C_p \left(\frac{\partial T}{\partial t} + u\frac{\partial T}{\partial x} + v\frac{\partial T}{\partial y}\right) &= \alpha_1 \left(\frac{\partial^2 u}{\partial y \partial t}\frac{\partial u}{\partial y} + u\frac{\partial^2 u}{\partial x \partial y}\frac{\partial u}{\partial y} + v\frac{\partial^2 u}{\partial y^2}\frac{\partial u}{\partial y}\right) + \\ & \mu\left(\frac{\partial u}{\partial y}\right)^2 - \frac{\partial}{\partial y}\left(\frac{16\sigma^* T_\infty^3}{3k^*} + k\right)\frac{\partial T}{\partial y} + \\ & \tau\left(D_B \frac{\partial C}{\partial y}\frac{\partial T}{\partial y} + \frac{D_T}{T_\infty}\left(\frac{\partial T}{\partial y}\right)^2\right). \end{aligned} \tag{7}$$

The imposed boundary conditions are given below

$$u = U_w, \quad v = V_w, \quad T = T_w, \quad C = C_w \quad at \quad y = 0, \tag{8}$$

$$u \to 0, \quad T \to T_\infty, \quad C \to C_\infty \quad as \ y \to \infty, \tag{9}$$

where

$$V_w = -\frac{v_0}{(1-ct)^{1/2}}, \tag{10}$$

is the mass transfer at surface with $V_w < 0$ for suction and $V_w > 0$ for injection. Moreover, the surface temperature $T_w(x, t)$, stretching velocity $U_w(x, t)$ and the value of nanoparticle volume fraction $C_w(x, t)$ are given by:

$$\begin{aligned} U_w(x,t) &= \frac{ax}{1-ct}, \quad T_w(x,t) = T_\infty + T_0\frac{ax}{2v(1-ct)^2}, \\ C_w(x,t) &= C_\infty + C_0\frac{ax}{2v(1-ct)^2}, \end{aligned} \tag{11}$$

with a and c are the constants with $a \geq 0$ and $c > 0$ (with $ct < 1$), and time^{-1} is the dimension for both a and c. We select unsteady magnetic field of the form $B(t) = B_0(1-ct)^{-1/2}$

Similarity transformation for the present case is given below

$$\begin{aligned} \eta &= \sqrt{\frac{U_w}{vx}}y, \qquad \psi = \sqrt{vxU_w}f(\eta), \\ \theta(\eta) &= \frac{T - T_\infty}{T_w - T_\infty}, \ \phi(\eta) = \frac{C - C_\infty}{C_w - C_\infty}, \end{aligned} \tag{12}$$

and the velocity components

$$u = \frac{\partial \psi}{\partial y}, \quad v = -\frac{\partial \psi}{\partial x}, \tag{13}$$

identically satisfies Eq (1) with stream function ψ while Eqs (2)–(4) and (7)–(9) are converted

into the following form

$$\begin{aligned} &f''' - f'^2 + ff'' - A\left(f' + \frac{\eta}{2}f''\right) - M^2 f' + \lambda(\theta + N\phi) + \\ &+\alpha\left(2f'f''' - f''^2 - ff'''' + A\left(2f''' + \frac{\eta}{2}f''''\right)\right) = 0, \end{aligned} \tag{14}$$

$$\begin{aligned} &\left(1 + \frac{4}{3}R_d\right)\theta'' + \Pr(f\theta' - f'\theta) + \Pr Ec(f'')^2 - \Pr\frac{A}{2}(\eta\theta' + 4\theta) + \\ &\Pr Ec\alpha\left(\frac{A}{2}\left(3(f'')^2 + \eta f''f'''\right) + f'f''^2 - ff''f'''\right) + \Pr\left(N_b\theta'\phi' + N_t\theta'^2\right) = 0, \end{aligned} \tag{15}$$

$$\phi'' + \left(\frac{N_t}{N_b}\right)\theta'' + \Pr Le(f\phi' - f'\phi) - \Pr LeA\left(2\phi + \frac{\eta}{2}\phi'\right) = 0, \tag{16}$$

$$\begin{aligned} f(0) &= S, \quad f'(0) = 1, \quad \theta(0) = 1, \quad \phi(0) = 1, \\ f'(\infty) &\to 0, \; f''(\infty) \to 0, \quad \theta(\infty) \to 0, \; \phi(\infty) \to 0. \end{aligned} \tag{17}$$

Here $A = a/c$ is the unsteadiness parameter, $\alpha = b\alpha_1/\mu\,(1-ct)$, (with $ct < 1$) is the second grade dimensionless parameter, $G_{r_x} = g\beta\,(T_w - T_\infty)x^3/\nu^2$ is the Grashof number, $\lambda = Gr_x/\mathrm{Re}_x^2$ is mixed convection parameter, $\mathrm{Re}_x = u_w\,x/\nu$ is the local Reynold number

$$\lambda = \frac{G_{r_x}}{Re_x^2}\left(= \frac{g\beta\,(T_w - T_\infty)\,x^3/\nu^2}{u_w^2 x^2/\nu^2}\right), \tag{18}$$

$Pr = \frac{\mu c_p}{k}$ is the Prandtl number, $R_D = \frac{4\sigma^* T_\infty^3}{3k^* k}$ is the radiation parameter, $Ec = \frac{u_w^2}{c_p(T_w - T_\infty)}$ is the Eckert number, $N_b = \frac{\tau D_B}{\nu}(C_w - C_\infty)$ is the Brownian motion parameter, $Nt = \frac{D_T}{T_\infty}\frac{\tau}{\nu}(T_w - T_\infty)$ is the thermophoresis, $Le = \frac{\alpha}{D_B}$ is the Lewis number.

The Skin friction coefficient, local Nusselt and local Sherwood numbers are given by the expressions

$$C_f = \frac{\tau_w}{\rho u_w^2}, \qquad Nu_x = \frac{xq_w}{k(T_w - T_\infty)}, \qquad Sh = \frac{x\,j_w}{D_B(C_w - C_\infty)}, \tag{19}$$

where the skin friction τ_w and wall heat flux q_w and the concentration flux j_w are defined as

$$\begin{aligned} \tau_w &= \left(\mu\frac{\partial u}{\partial y} + \alpha_1\left(\frac{\partial^2 u}{\partial y\partial t} + 2\frac{\partial u}{\partial x}\frac{\partial u}{\partial y} + u\frac{\partial^2 u}{\partial x\partial y} + \nu\frac{\partial^2 u}{\partial y^2}\right)\right)_{y=0}, \\ q_w &= -k\left(\frac{\partial T}{\partial r}\right)_{y=0}, \quad j_w = -D_B\left(\frac{\partial C}{\partial r}\right)_{r=0}. \end{aligned} \tag{20}$$

Dimensionless forms of skin friction coefficient, local Nusselt and local Sherwood numbers are

$$\begin{aligned} C_f Re_x^{1/2} &= \left(f''(\eta) + \alpha\begin{pmatrix} 3f'(\eta)f''(\eta) - f(\eta)f'''(\eta) + \\ \frac{A}{2}\left(3f''(\eta) + \eta f'''(\eta)\right) \end{pmatrix}\right)_{\eta=0}, \\ N_{u_x} Re_x^{-1/2} &= -\theta'(0), \qquad\qquad Sh Re_x^{-1/2} = -\phi'(0), \end{aligned} \tag{21}$$

where $\mathrm{Re}_z = w_e\,z/\nu$ is the Reynolds number.

Homotopic solutions

The initial guesses and the auxiliary linear operators are essential for the homotopic solutions. The initial guesses and the auxiliary linear operators for the present flow problems are

$$f_0(\eta) = S + (1 - \exp(-\eta)), \qquad \theta_0(\eta) = \exp(-\eta), \qquad \phi_0(\eta) = \exp(-\eta). \tag{22}$$

$$\mathcal{L}_f(\eta) = \frac{d^3 f}{d\eta^3} - \frac{df}{d\eta}, \ \mathcal{L}_\theta(\eta) = \frac{d^2\theta}{d\eta^2} - \theta, \ \mathcal{L}_\phi(\eta) = \frac{d^2\phi}{d\eta^2} - \phi. \tag{23}$$

The auxiliary linear operators have the following properties

$$\mathcal{L}_f[C_1 + C_2 \exp(\eta) + C_3 \exp(-\eta)] = 0, \tag{24}$$

$$\mathcal{L}_\theta[C_4 \exp(\eta) + C_5 \exp(-\eta)] = 0, \tag{25}$$

$$\mathcal{L}_\phi[C_6 \exp(\eta) + C_7 \exp(-\eta)] = 0, \tag{26}$$

where C_i (i = 1–7) are the arbitrary constants. The zeroth and mth order deformation problems are stated below.

Zeroth-order problem

The problems at zeroth order deformation can be expressed as

$$(1-p)\mathcal{L}_f\left[\hat{f}(\eta;p) - f_0(\eta)\right] = p\hbar_f \mathcal{N}_f\left[\hat{f}(\eta;p), \hat{\theta}(\eta;p), \hat{\phi}(\eta;p)\right], \tag{27}$$

$$(1-p)\mathcal{L}_\theta\left[\hat{\theta}(\eta;p) - \theta_0(\eta)\right] = p\hbar_\theta \mathcal{N}_\theta\left[\hat{\theta}(\eta;p), \hat{f}(\eta;p), \hat{\phi}(\eta;p)\right], \tag{28}$$

$$(1-p)\mathcal{L}_\phi\left[\hat{\phi}(\eta;p) - \phi_0(\eta)\right] = p\hbar_\phi \mathcal{N}_\phi\left[\hat{\phi}(\eta;p), \hat{f}(\eta;p), \hat{\theta}(\eta;p)\right], \tag{29}$$

$$\hat{f}(\eta;p)\Big|_{\eta=0} = S, \qquad \frac{\partial \hat{f}(\eta;p)}{\partial \eta}\Big|_{\eta=0} = 1, \qquad \frac{\partial \hat{f}(\eta;p)}{\partial \eta}\Big|_{\eta=\infty} = 1, \tag{30}$$

$$\hat{\theta}(\eta;p)\Big|_{\eta=0} = 1, \qquad \hat{\theta}(\eta;p)\Big|_{\eta=\infty} = 0, \tag{31}$$

$$\hat{\phi}(\eta;p)\Big|_{\eta=0} = 1, \qquad \hat{\phi}(\eta;p)\Big|_{\eta=\infty} = 0, \tag{32}$$

$$\begin{aligned}\mathcal{N}_f(\hat{f}(\eta,p),\hat{\theta}(\eta;p),\hat{\phi}(\eta;p)) &= \frac{\partial^3\hat{f}(\eta;p)}{\partial\eta^3}+\hat{f}(\eta;p)\frac{\partial^2\hat{f}(\eta;p)}{\partial\eta^2}-\left(\frac{\partial\hat{f}(\eta;p)}{\partial\eta}\right)^2\\ &\quad -M^2\frac{\partial\hat{f}(\eta;p)}{\partial\eta}-A\left(\frac{\eta}{2}\frac{\partial^2\hat{f}(\eta;p)}{\partial\eta^2}+\frac{\partial\hat{f}(\eta;p)}{\partial\eta}\right)+\\ &\quad \alpha\left(\begin{array}{c}-\left(\frac{\partial^2\hat{f}(\eta;p)}{\partial\eta^2}\right)^2-A\left(2\frac{\partial^3\hat{f}(\eta;p)}{\partial\eta^3}+\frac{\eta}{2}\frac{\partial^4\hat{f}(\eta;p)}{\partial\eta^4}\right)\\ +2\frac{\partial\hat{f}(\eta;p)}{\partial\eta}\frac{\partial^3\hat{f}(\eta;p)}{\partial\eta^3}-\frac{\partial\hat{f}(\eta;p)}{\partial\eta}\frac{\partial^4\hat{f}(\eta;p)}{\partial\eta^4}\end{array}\right)+\\ &\quad \lambda(\hat{\theta}(\eta;p)+N\hat{\phi}(\eta;p))+\lambda\hat{\theta}(\eta;p),\end{aligned} \tag{33}$$

$$\begin{aligned}\mathcal{N}_\theta(\hat{\theta}(\eta;p),\hat{f}(\eta;p),\hat{\phi}(\eta;p)) &= \left(1+\frac{4}{3}R_d\right)\frac{\partial^2\hat{\theta}(\eta,p)}{\partial\eta^2}+\\ &\quad \Pr\left(\hat{f}(\eta;p)\frac{\partial\hat{\theta}(\eta;p)}{\partial\eta}-\frac{\partial\hat{f}(\eta;p)}{\partial\eta}\hat{\theta}(\eta,p)\right)+\\ &\quad \Pr Ec\left(\frac{\partial^2\hat{f}(\eta;p)}{\partial\eta^2}\right)^2-\Pr\frac{A}{2}\left(\eta\frac{\partial\hat{\theta}(\eta;p)}{\partial\eta}+4\hat{\theta}(\eta;p)\right)+\\ &\quad \Pr Ec\alpha\left(\begin{array}{c}\frac{A}{2}\left(3\left(\frac{\partial^2\hat{f}(\eta;p)}{\partial\eta^2}\right)^2+\eta\frac{\partial^2\hat{f}(\eta;p)}{\partial\eta^2}\frac{\partial^3\hat{f}(\eta;p)}{\partial\eta^3}\right)\\ +\frac{\partial\hat{f}(\eta;p)}{\partial\eta}\left(\frac{\partial^2\hat{f}(\eta;p)}{\partial\eta^2}\right)^2\\ -\hat{f}(\eta;p)\frac{\partial^2\hat{f}(\eta;p)}{\partial\eta^2}\frac{\partial^3\hat{f}(\eta;p)}{\partial\eta^3}\end{array}\right)\\ &\quad +\Pr\left(N_b\frac{\partial\hat{\theta}(\eta;p)}{\partial\eta}\frac{\partial\hat{\phi}(\eta,p)}{\partial\eta}+N_t\left(\frac{\partial\hat{\theta}(\eta,p)}{\partial\eta}\right)^2\right),\end{aligned} \tag{34}$$

$$\begin{aligned}\mathcal{N}_\phi(\hat{\phi}(\eta;p),\hat{f}(\eta;p),\hat{\theta}(\eta;p)) &= \frac{\partial^2\hat{\phi}(\eta,p)}{\partial\eta^2}+\Pr Le\left(\hat{f}(\eta;p)\frac{\partial\hat{\phi}(\eta;p)}{\partial\eta}-\frac{\partial\hat{f}(\eta;p)}{\partial\eta}\hat{\phi}(\eta,p)\right)\\ &\quad -\Pr Le\left(A\left(2\hat{\phi}(\eta;p)+\frac{\eta}{2}\frac{\partial\hat{\phi}(\eta,p)}{\partial\eta}\right)\right)+\frac{N_t}{N_b}\frac{\partial^2\hat{\theta}(\eta,p)}{\partial\eta^2}.\end{aligned} \tag{35}$$

For p = 0 and p = 1, we have

$$\hat{f}(\eta;0)=f_0(\eta),\quad \hat{f}(\eta;1)=f(\eta), \tag{36}$$

$$\hat{\theta}(\eta;0)=\theta_0(\eta),\quad \hat{\theta}(\eta;1)=\theta(\eta), \tag{37}$$

$$\hat{\phi}(\eta;0)=\phi_0(\eta),\quad \hat{\phi}(\eta;1)=\phi(\eta), \tag{38}$$

and when p increases from 0 to 1, then $\hat{f}(\eta;p)$, $\hat{\theta}(\eta;p)$ and $\hat{\phi}(\eta;p)$ changes from $f_0(\eta)$, $\theta_0(\eta)$ and $\phi_0(\eta)$, the initial guess, to $f(\eta)$, $\theta(\eta)$ and $\phi(\eta)$, the final solutions, respectively. Expanding

$\hat{f}(\eta;p), \hat{\theta}(\eta;p)$ and $\hat{\phi}(\eta;p)$ we have

$$\hat{f}(\eta;p) = f_0(\eta) + \sum_{m=1}^{\infty} f_m(\eta)p^m, \tag{39}$$

$$\hat{\theta}(\eta;p) = \theta_0(\eta) + \sum_{m=1}^{\infty} \theta_m(\eta)p^m, \tag{40}$$

$$\hat{\phi}(\eta;p) = \phi_0(\eta) + \sum_{m=1}^{\infty} \phi(\eta)p^m. \tag{41}$$

*m*th-order deformation problems

$$\mathcal{L}_f[f_m(\eta) - \chi_m f_{m-1}(\eta)] = \hbar_f \mathcal{R}_m^f(\eta), \tag{42}$$

$$\mathcal{L}_\theta[\theta_m(\eta) - \chi_m \theta_{m-1}(\eta)] = \hbar_\theta \mathcal{R}_m^\theta(\eta), \tag{43}$$

$$\mathcal{L}_\phi[\phi_m(\eta) - \chi_m \phi_{m-1}(\eta)] = \hbar_\phi \mathcal{R}_m^\phi(\eta), \tag{44}$$

$$f_m(0) = f_m'(0) = f_m'(\infty) = 0, \tag{45}$$

$$\theta_m(0) = \theta_m(\infty) = 0, \tag{46}$$

$$\phi_m(0) = \phi_m(\infty) = 0, \tag{47}$$

$$\begin{aligned} \mathcal{R}_m^f(\eta) &= f_{m-1}''' - A\left(f_{m-1}' + \frac{1}{2}\eta f_{m-1}''\right) + \alpha A\left(2f_{m-1}''' + \frac{1}{2}\eta f_{m-1}''''\right) - M^2 f_{m-1}' + \\ &\quad \sum_{k=0}^{m-1}\left[f_{m-1-k}f_k'' - f_{m-1-k}'f_k' + \alpha(2f_{m-1-k}f_k''' - f_{m-1-k}''f_k'' - f_{m-1-k}f_k'''')\right] \\ &\quad + \lambda(\theta_{m-1-k} + N\phi_{m-1-k}), \end{aligned} \tag{48}$$

$$\begin{aligned} \mathcal{R}_m^\theta(\eta) &= \left(1 + \frac{4}{3}R_d\right)\theta_{m-1}'' - \Pr\frac{A}{2}\left(\eta\theta_{m-1}' + 4\theta_{m-1-k}\right) + \Pr\sum_{k=0}^{m-1}\left(f_{m-1-k}\theta_k' - f_{m-1-k}'\theta_k\right) \\ &\quad + \Pr Ec\left[\sum_{k=0}^{m-1}\left[f_{m-1-k}'f_k'' + \alpha\left(\begin{array}{c}\frac{A}{2}\left(3f_{m-1-k}''f_k'' + \eta f_{m-1-k}''f_k'''\right) \\ + f_{m-1-k}'\sum_{k=0}^{m-1}f_{k-l}''f_l'' - f_{m-1-k}\sum_{k=0}^{m-1}f_{k-l}''f_l'''\end{array}\right)\right]\right] \\ &\quad \Pr\left(N_b\sum_{k=0}^{m-1}(\theta_{m-1-k}'\phi_k - \theta_{m-1-k}'\theta_k') + N_t\sum_{k=0}^{m-1}(f_{m-1-k}\theta_k' - f_{m-1-k}'\theta_k)\right), \end{aligned} \tag{49}$$

$$\mathcal{R}_m^{\phi}(\eta) = \phi''_{m-1} + 2\gamma\phi'_{m-1} + \Pr Le\sum_{k=0}^{m-1}\left(f_{m-1-k}\phi'_k - f'_{m-1-k}\phi_k\right) + \frac{N_t}{N_b}\theta''_{m-1} - \Pr Le\left[A\left(2\phi_{m-1-k} + \frac{\eta}{2}\phi'_{m-1}\right)\right], \tag{50}$$

$$\chi_m = \begin{cases} 0, & m \le 1 \\ 1, & m > 1 \end{cases}. \tag{51}$$

The general solutions of the Equations are

$$f_m(\eta) = f_m^*(\eta) + C_1 + C_2\exp(\eta) + C_3\exp(\eta), \tag{52}$$

$$\theta_m(\eta) = \theta_m^*(\eta) + C_4\exp(\eta) + C_5\exp(\eta), \tag{53}$$

$$\phi_m(\eta) = \phi_m^*(\eta) + C_6\exp(\eta) + C_7\exp(\eta). \tag{54}$$

For $p = 0$ and $p = 1$, we have

$$\hat{f}(\eta;0) = f_0(\eta), \quad \hat{f}(\eta;1) = f(\eta), \tag{55}$$

$$\hat{\theta}(\eta;0) = \theta_0(\eta), \quad \hat{\theta}(\eta;1) = \theta(\eta), \tag{56}$$

$$\hat{\phi}(\eta;0) = \phi_0(\eta), \quad \hat{\phi}(\eta;1) = \phi(\eta), \tag{57}$$

and with the variation of p from 0 to 1, $\hat{f}(\eta;p)$, $\hat{\theta}(\eta;p)$ and $\hat{\phi}(\eta;p)$ vary from the initial solutions $f_0(\eta)$, $\theta_0(\eta)$ and $\phi_0(\eta)$ to the final solutions $f(\eta)$, $\theta(\eta)$ and $\phi(\eta)$ respectively. By Taylor's series we have

$$\hat{f}(\eta;p) = f_0(\eta) + \sum_{m=1}^{\infty} f_m(\eta)p^m, \quad f_m(\eta) = \frac{1}{m!}\frac{\partial^m\hat{f}(\eta;p)}{\partial p^m}\bigg|_{p=0}, \tag{58}$$

$$\hat{\theta}(\eta;p) = \theta_0(\eta) + \sum_{m=1}^{\infty} \theta_m(\eta)p^m, \quad \theta_m(\eta) = \frac{1}{m!}\frac{\partial^m\hat{\theta}(\eta;p)}{\partial p^m}\bigg|_{p=0}, \tag{59}$$

$$\hat{\phi}(\eta;p) = \phi_0(\eta) + \sum_{m=1}^{\infty} \phi_m(\eta)p^m, \quad \phi_m(\eta) = \frac{1}{m!}\frac{\partial^m\hat{\phi}(\eta;p)}{\partial p^m}\bigg|_{p=0}. \tag{60}$$

The value of auxiliary parameter is chosen in such a way that the series (43)–(45) converge at $p = 1$ i.e.,

$$f(\eta) = f_0(\eta) + \sum_{m=1}^{\infty} f_m(\eta), \tag{61}$$

$$\theta(\eta) = \theta_0(\eta) + \sum_{m=1}^{\infty} \theta_m(\eta), \tag{62}$$

$$\phi(\eta) = \phi_0(\eta) + \sum_{m=1}^{\infty} \phi_m(\eta). \tag{63}$$

The general solutions (f_m, θ_m, ϕ_m) of Eqs (30)–(32) in terms of special solutions $\left(f_m^*, \theta_m^*, \phi_m^*\right)$ are given by

$$f_m(\eta) = f_m^\star(\eta) + A_1 + A_2 e^{\eta} + A_3 e^{-\eta}, \tag{64}$$

$$\theta_m(\eta) = \theta_m^\star(\eta) + A_4 e^{\eta} + A_5 e^{-\eta}, \tag{65}$$

$$\phi_m(\eta) = \phi_m^\star(\eta) + A_6 e^{\eta} + A_7 e^{-\eta}, \tag{66}$$

in above expressions, $f_m^*(\eta), \theta_m^*(\eta)$ and $\phi_m^*(\eta)$ denotes the special functions and the constants A_i (i = 1–7) through the boundary conditions have the values

$$\begin{aligned} A_2 &= A_4 = A_6 = 0, \qquad A_3 = \left.\frac{\partial f_m^\star(\eta)}{\partial \eta}\right|_{\eta=0}, \qquad A_1 = -A_3 - f_m^\star(0), \\ A_5 &= -\theta_m^*(0),\ A_7 = -\phi_m^*(0). \end{aligned} \tag{67}$$

Convergence of solution

To find the meaningful series solutions of momentum, energy and concentration equations, the convergence region is essential to determine. Convergence region of the series solutions depend upon the auxiliary parameter $\hbar$. Therefore we have plotted the $\hbar$-curves in the Fig 2. The

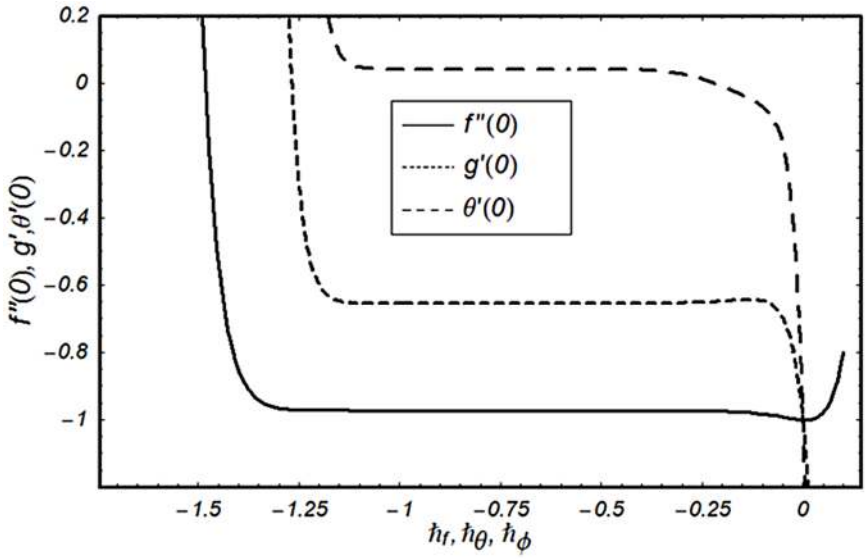

Fig 2. $\hbar$-curve for function f, θ, ϕ.

doi:10.1371/journal.pone.0124929.g002

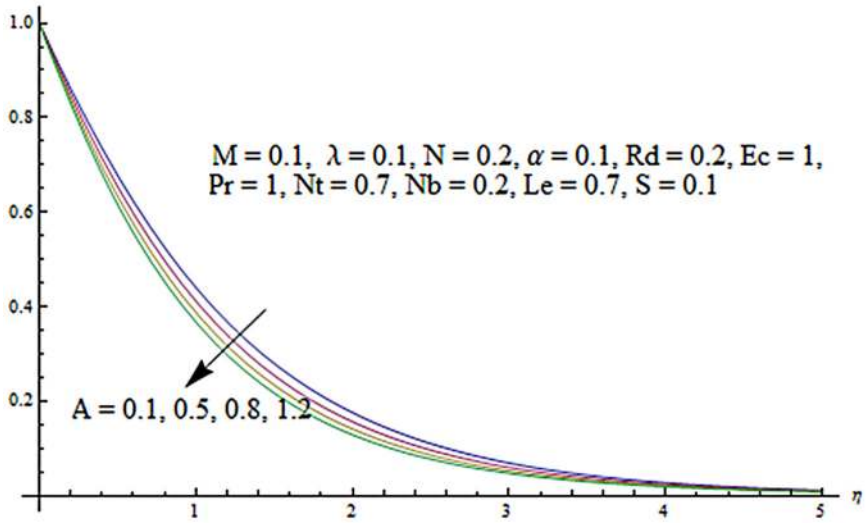

Fig 3. Influence of *A* on *θ*.

doi:10.1371/journal.pone.0124929.g003

tolerable range for admissible values of the auxiliary parameters $\hbar_f$, $\hbar_\theta$ and $\hbar_\phi$ are $-1.1 \leq \hbar_f \leq -0.5$, $-1.1 \leq \hbar_\theta \leq -0.5$ and $-1.1 \leq \hbar_\phi \leq -0.45$.

Figs 3 and 4 presents the influence of unsteady parameter A on the temperature profile $\theta(\eta)$ and nanoparticle concentration $\phi(\eta)$. It is observed that an increase in unsteady parameter creates a reduction in the temperature and nanoparticle concentration profiles. Effects of Hartman number M on temperature and nanoparticle concentration fields are examined in Figs 5 and 6.

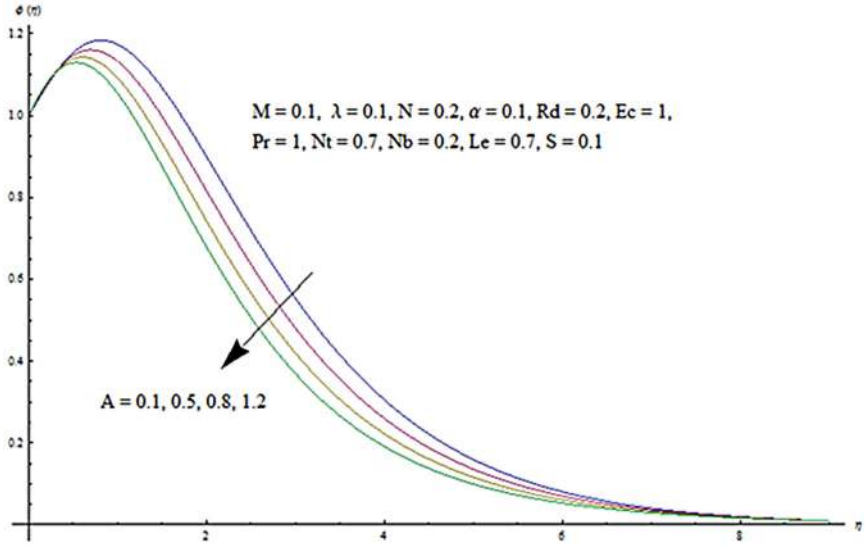

Fig 4. Influence of *A* on ϕ.

doi:10.1371/journal.pone.0124929.g004

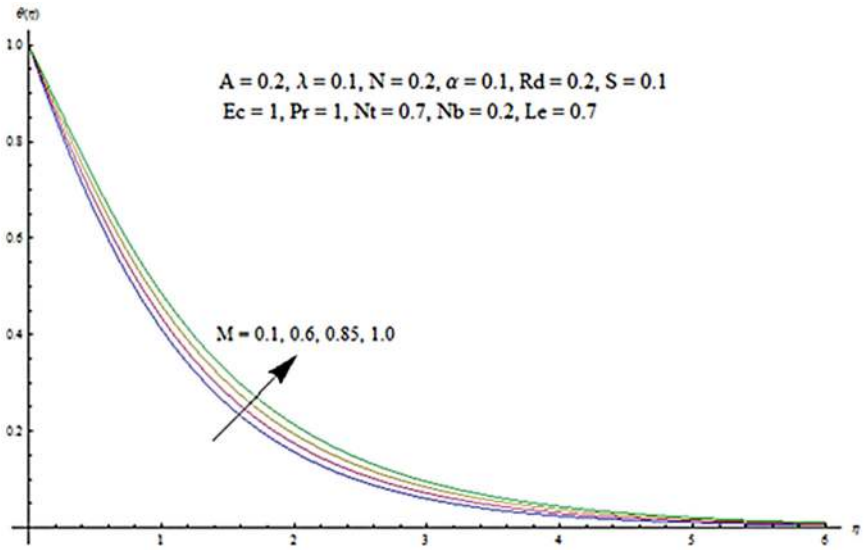

Fig 5. Influence of *M* on *θ*.

doi:10.1371/journal.pone.0124929.g005

Here we have observed that both temperature and nanoparticle concentration fields are enhanced with an increase in Hartman number. Physically, Hartman number involves the Lorentz force. This Lorentz force is stronger for the larger Hartman number due to which the temperature and nanoparticle concentration are increased. To examine the effects of second grade parameter α on the temperature and nanoparticle concentration profiles, we plotted the Figs 7 and 8. These figs. clearly show that an increase in second grade parameter gives rise to

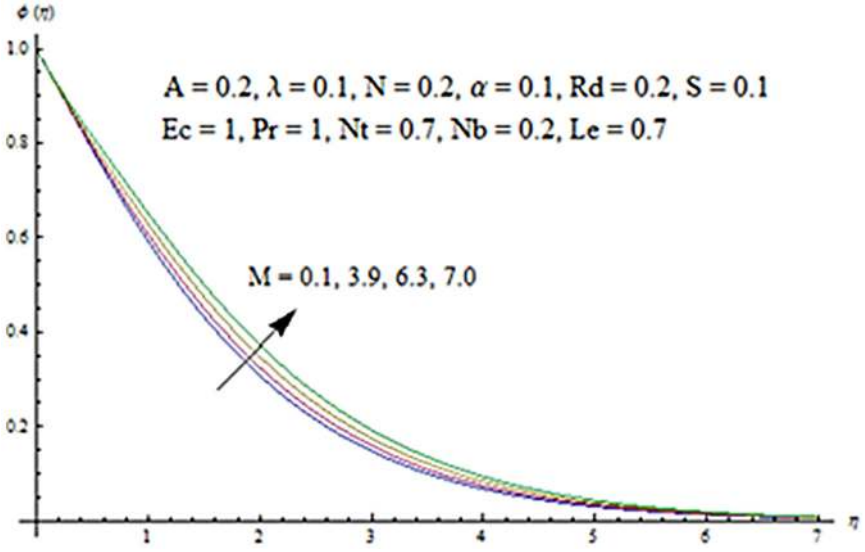

Fig 6. Influence of *M* on ϕ.

doi:10.1371/journal.pone.0124929.g006

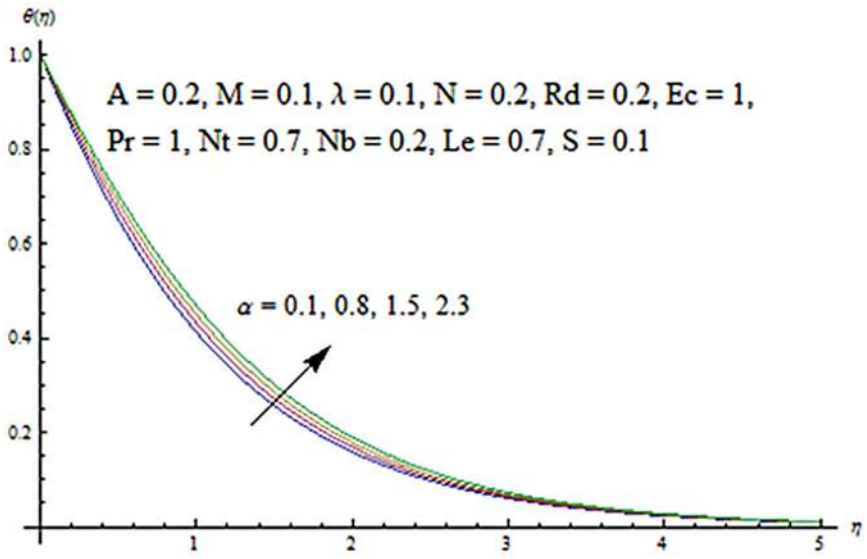

Fig 7. Influence of α on θ.

doi:10.1371/journal.pone.0124929.g007

the temperature and thermal boundary layer thickness but a decrease is seen for the nanoparticle concentration profiles. Figs 9 and 10 depicts the variation in temperature and nanoparticle concentration profiles for different values of suction parameter *S*. An increase in suction parameter corresponds to a lower temperature and nanoparticle concentration profiles. Here suction parameter works as an agent which leads to a reduction in both temperature and nanoparticle concentration profiles. From Figs 11 and 12, we observe that both temperature

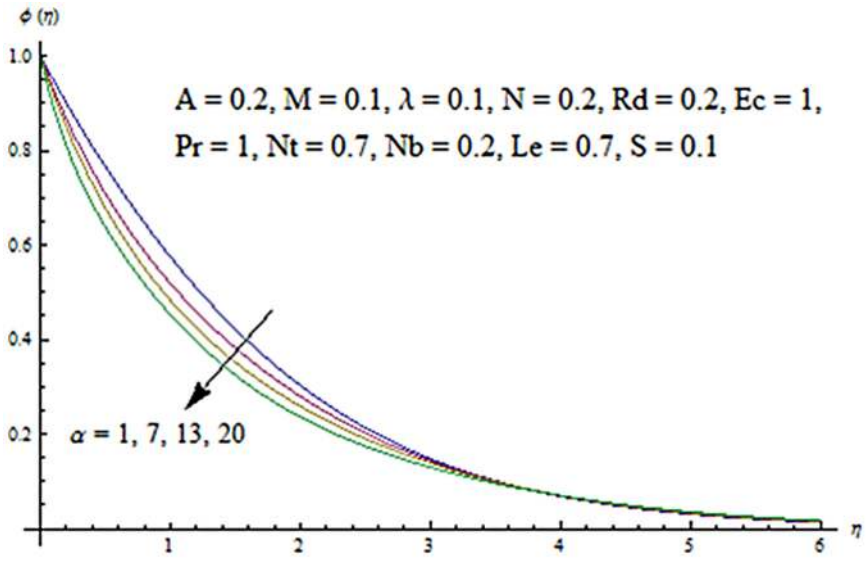

Fig 8. Influence of α on ϕ.

doi:10.1371/journal.pone.0124929.g008

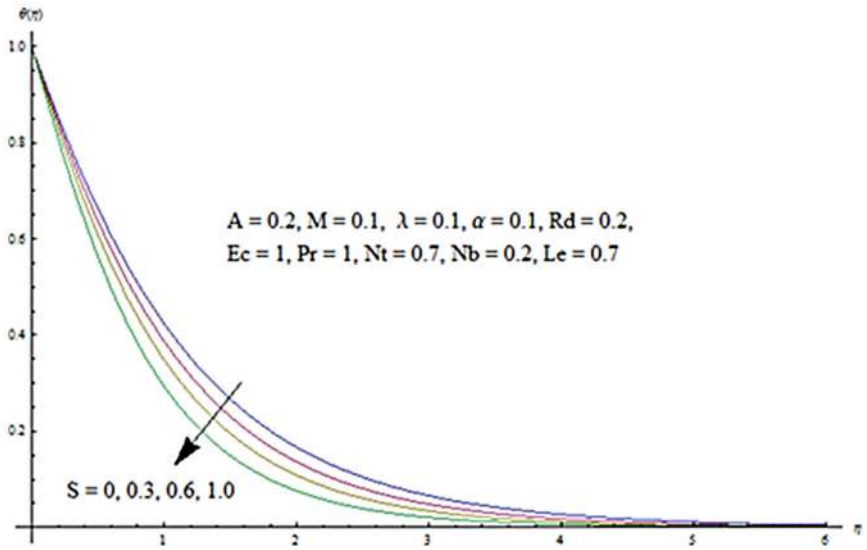

Fig 9. Influence of *S* on *θ*.

doi:10.1371/journal.pone.0124929.g009

and nanoparticle concentration fields are decreased when the values of buoyancy parameter λ are increased. It is due to the reason that buoyancy parameter has buoyancy force. This buoyancy force is stronger for larger buoyancy parameter. Such stronger buoyancy force leads a reduction in the temperature and nanoparticle concentration.

Figs 13 and 14 are presented to see the change in temperature and nanoparticle concentration corresponding to different values of *Pr*. From these figs. we analyzed that an increase in

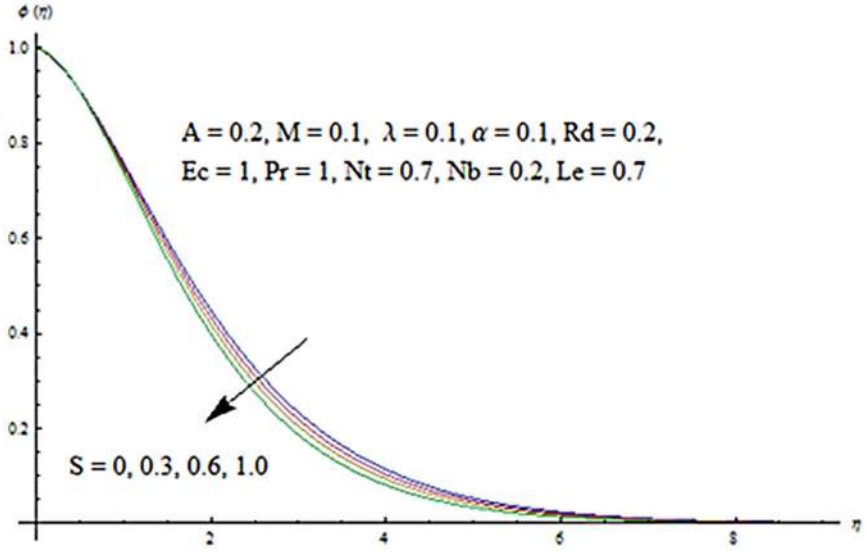

Fig 10. Influence of *S* on ϕ.

doi:10.1371/journal.pone.0124929.g010

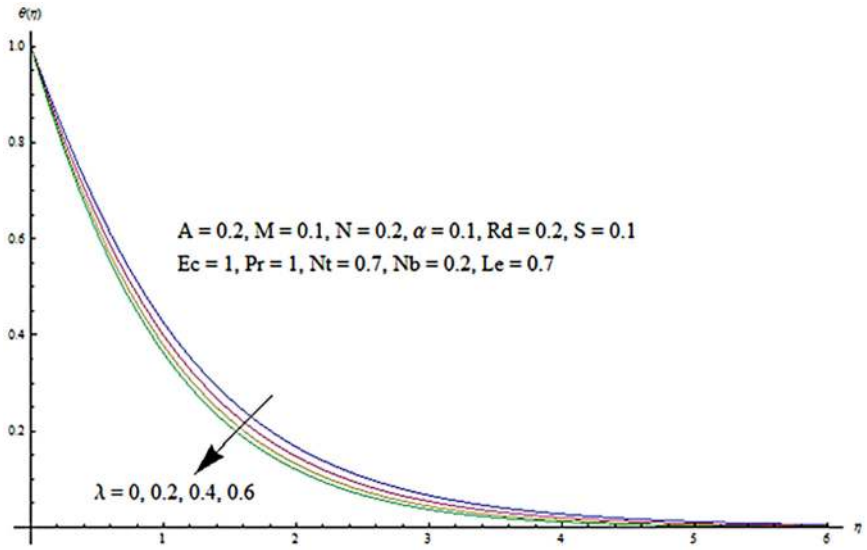

Fig 11. Influence of λ on θ.

doi:10.1371/journal.pone.0124929.g011

Prandtl number shows thinner thermal and nanoparticle concentration boundary layer thickness. Larger Prandtl number fluids have lower thermal diffusivity. Due to the lower thermal diffusivity, thinner thermal and nanoparticle concentration boundary layer thicknesses are observed. From Figs 15 and 16, it is seen that the larger values of Eckert number *Ec* corresponds to higher temperature and nanoparticle concentration. With an enhancement in value of Eckert number, we see an increase in kinetic energy due to which the temperature and nanoparticle

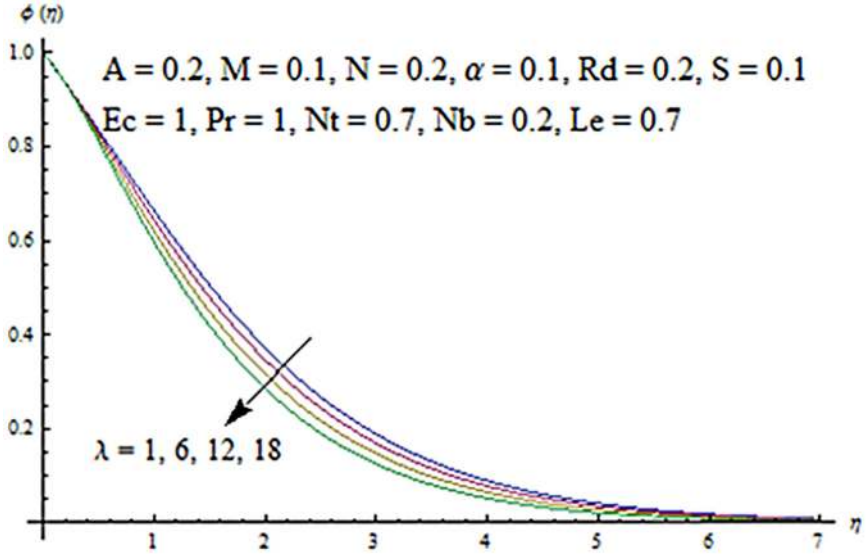

Fig 12. Influence of λ on ϕ.

doi:10.1371/journal.pone.0124929.g012

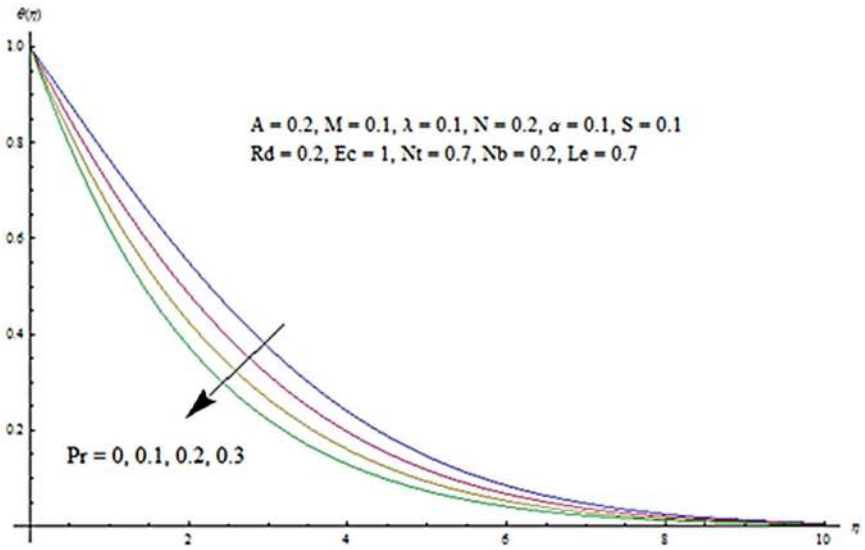

Fig 13. Influence of Pr on θ.

doi:10.1371/journal.pone.0124929.g013

concentration are enhanced. Influence of thermophoresis parameter *Nt* on temperature and nanoparticle concentration profiles is studied in the Figs 17 and 18. From these figs. we noted that an enhancement in thermophoresis parameter give rise to the temperature and nanoparticle concentration profiles. The variations in nanoparticle concentration profile are more pronounced in comparison to the temperature field due to an increase in thermophoresis parameter. Figs 19 and 20 illustrate that both temperature and nanoparticle concentration

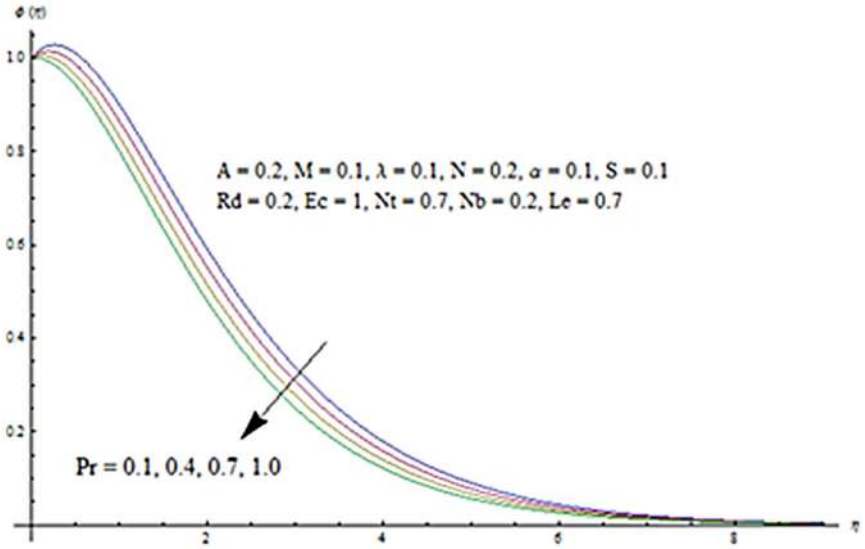

Fig 14. Influence of Pr on ϕ.

doi:10.1371/journal.pone.0124929.g014

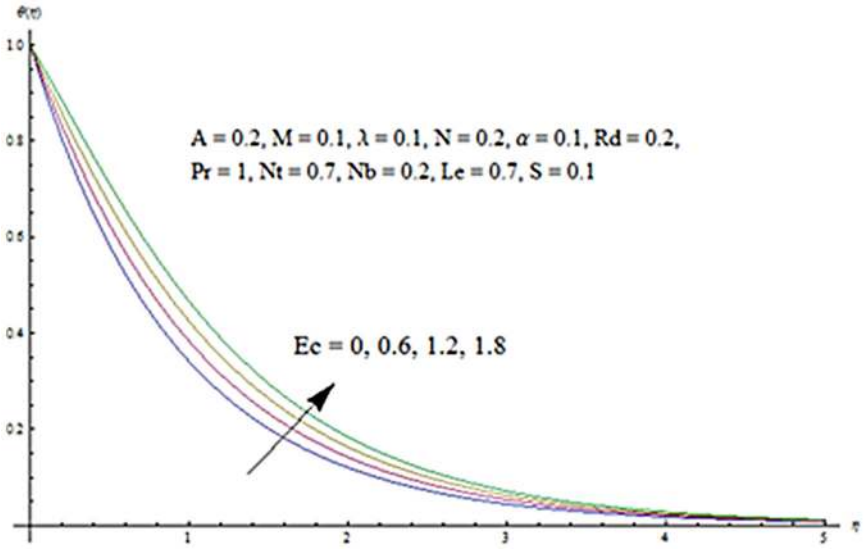

Fig 15. Influence of *Ec* on *θ*.

doi:10.1371/journal.pone.0124929.g015

profiles are quit opposite due to an enhancement in Brownian motion parameter. An increase in Lewis number *Le* shows an increase in temperature and decrease in nanoparticle concentration profile. (see Figs 21 and 22). The variation of suction parameter *S* on velocity f' is shown in Fig 23. It is observed that velocity and boundary layer thickness decrease with an increase in values of *S*. In practical, the porosity of wall controls the boundary layer flow. Fig 24 depicts that f' is a decreasing function of *M* because increasing the value of *M* results in an increase in Lorentz force thus decrease the magnitude of velocity.

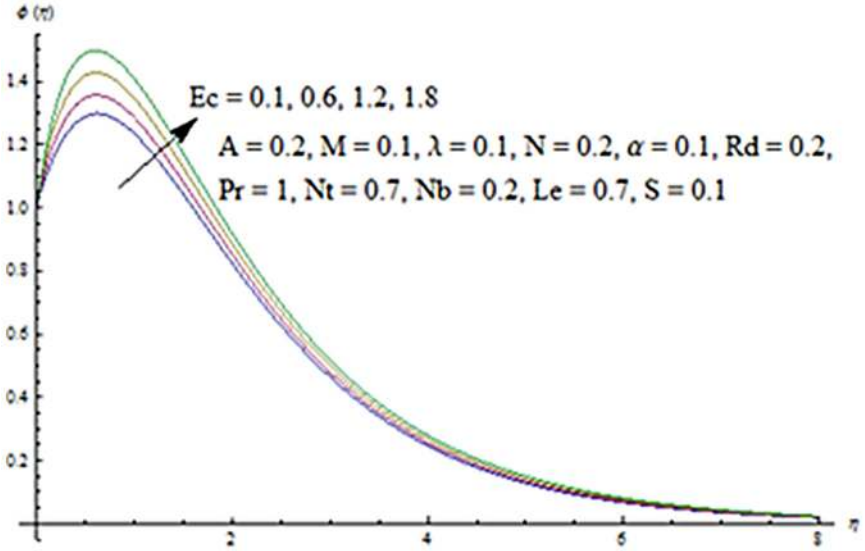

Fig 16. Influence of *Ec* on ϕ.

doi:10.1371/journal.pone.0124929.g016

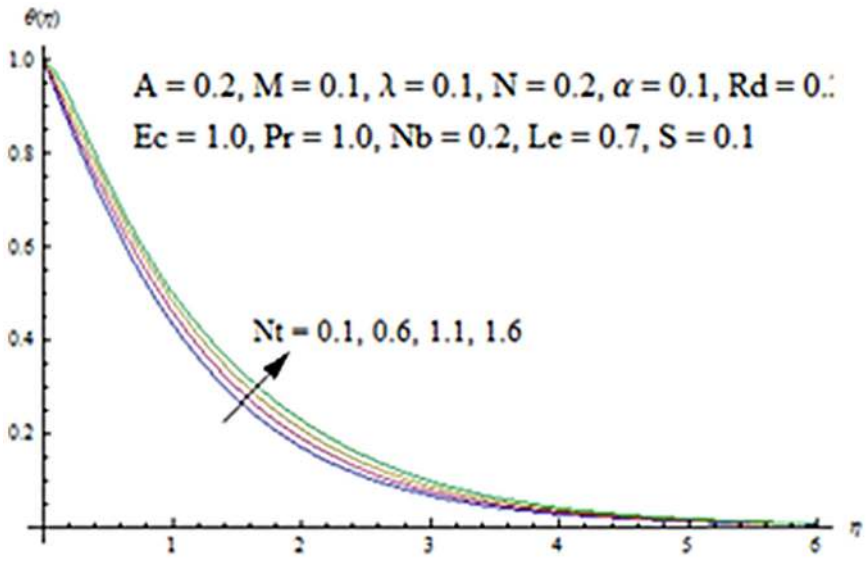

Fig 17. Influence of *Nt* on *θ*.

doi:10.1371/journal.pone.0124929.g017

Table 1 gives the convergent values of $f''(0)$, $\theta'(0)$ and $\phi'(0)$ at different order of HAM deformations. Here it is seen that the values of $f''(0)$ converges from 10-th order of deformations while the values of $\theta'(0)$ and $\phi'(0)$ repeats from 13-th and 16-th order of computations. Hence the 16-th order of HAM computations is essentials for the convergent homotopic solutions. Table 2 presents the numerical values of skin-friction coefficient, local Nusselt and Sherwood numbers for different values of A, M, λ, N, α and Rd when $Pr = 1 = Ec$, $Nt = 0.7$, $Nb = 0.2$,

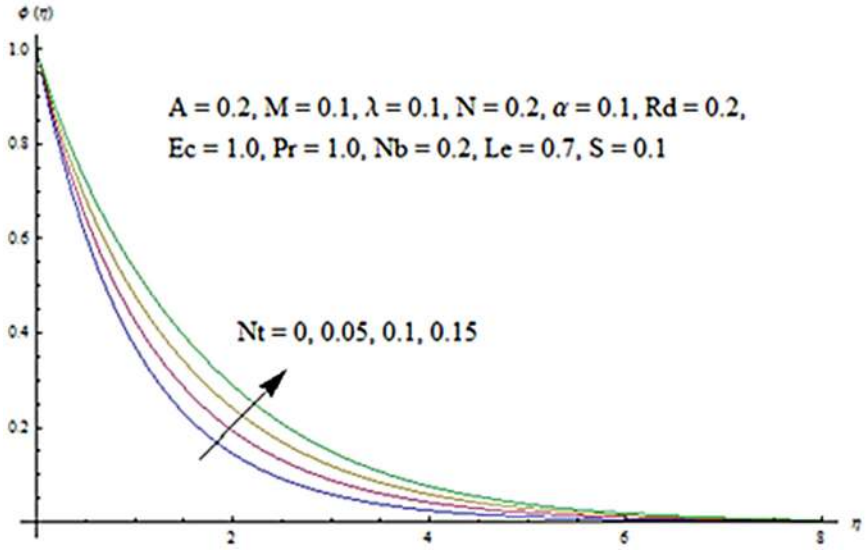

Fig 18. Influence of *Nt* on ϕ.

doi:10.1371/journal.pone.0124929.g018

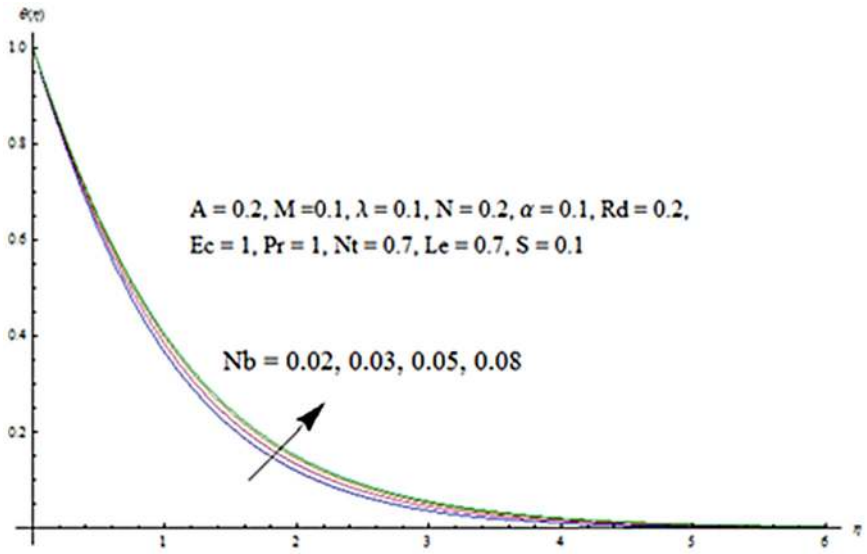

Fig 19. Influence of *Nb* on *θ*.

doi:10.1371/journal.pone.0124929.g019

$Le = 0.7$ and $S = 0.1$. From this table, it is examined that the values of skin-friction coefficient are increased with an increase in N but the values of Nusselt and Sherwood number are reduced. The values of Skin-friction coefficient, local Nusselt and Sherwood numbers for different values of Pr, Nb, Nt, Le and S when $A = 0.2$, $M = 0.1$, $\lambda = 0.1$, $\alpha = 0.1$, $N = 0.2$ and $Rd = 0.2$ are studied in Table 3. The numerical values of skin-friction coefficient, local Nusselt and Sherwood numbers are enhanced with an increase in the value of Pr. The Nomenclature of all parameters used is depicted in Table 4.

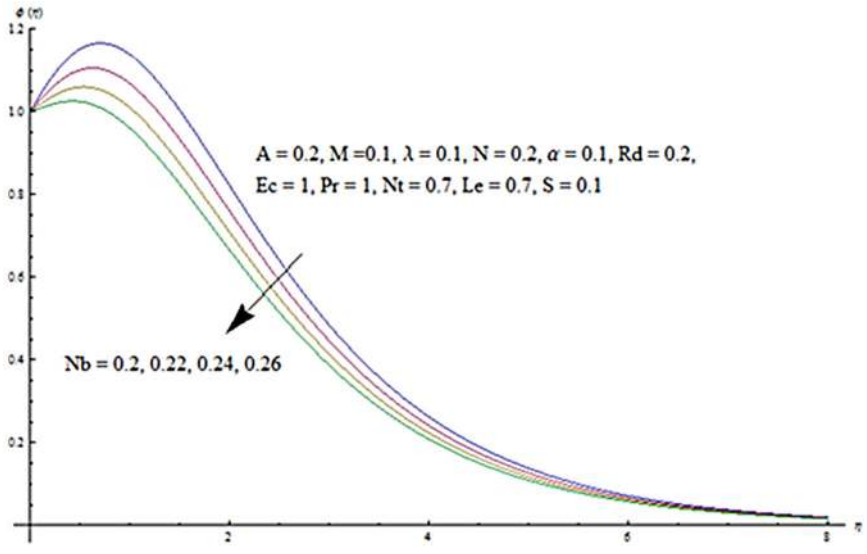

Fig 20. Influence of *Nb* on ϕ.

doi:10.1371/journal.pone.0124929.g020

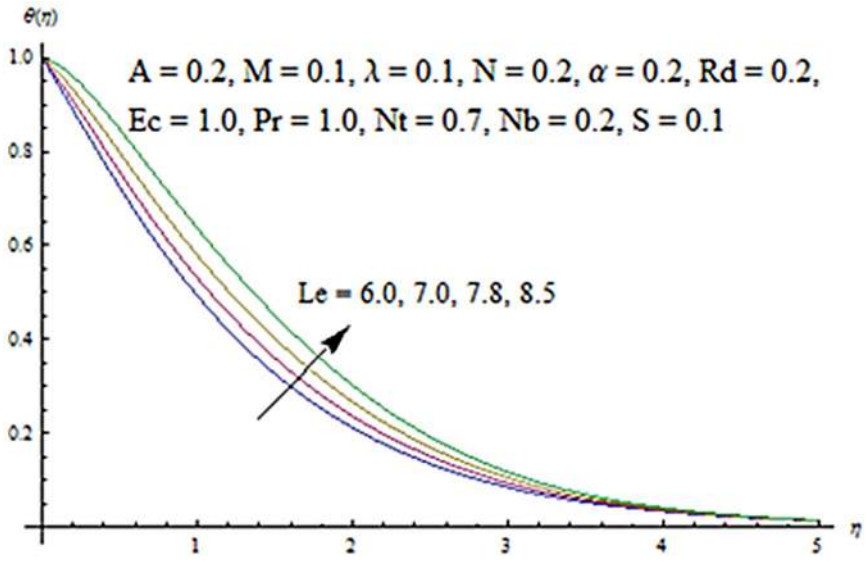

Fig 21. Influence of *Le* on *θ*.

doi:10.1371/journal.pone.0124929.g021

Final remarks

Unsteady MHD flow of second grade nanofluid induced by vertical sheet with mixed convection and thermal radiation is examined by Homotopy analysis method. The behavior of arised parameters have been discussed. The salient features of this exploration are appended below.

- The influence of Hartman number M, second grade dimensionless parameter α and Eckert number Ec on θ are similar.

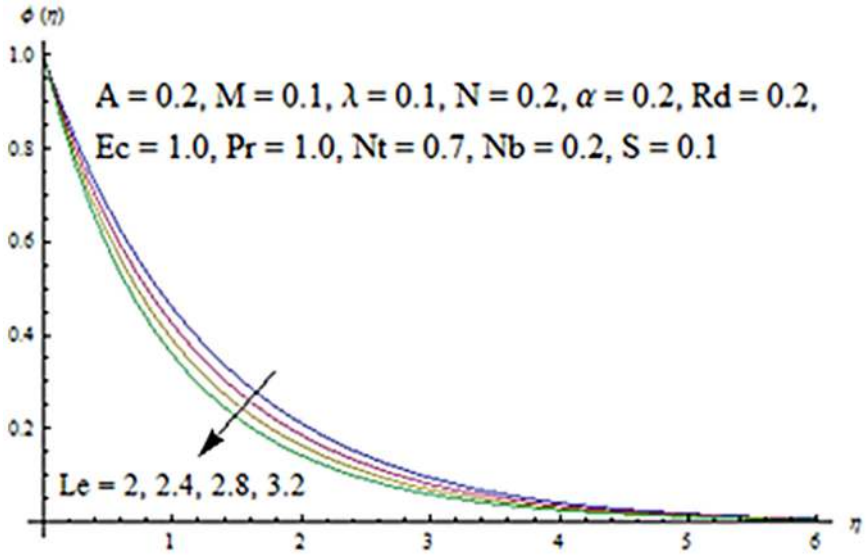

Fig 22. Influence of *Le* on ϕ.

doi:10.1371/journal.pone.0124929.g022

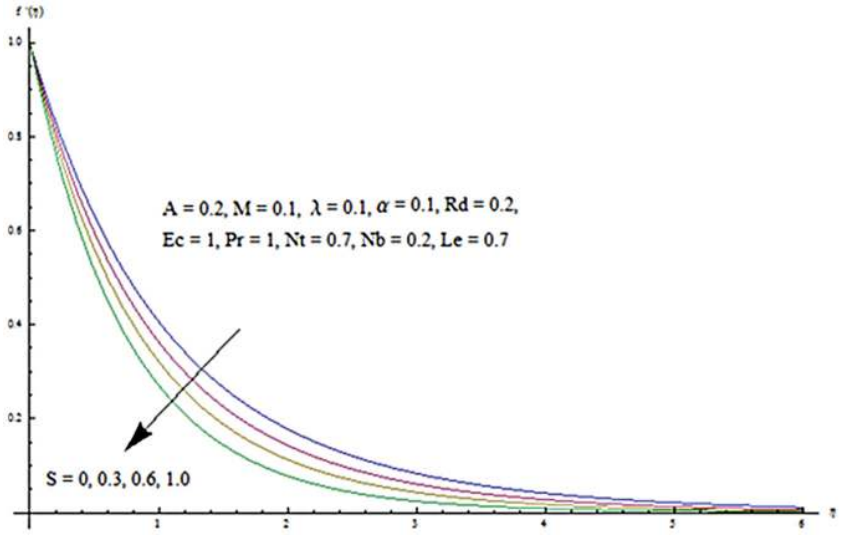

Fig 23. Influence of *S* on *f′*.

doi:10.1371/journal.pone.0124929.g023

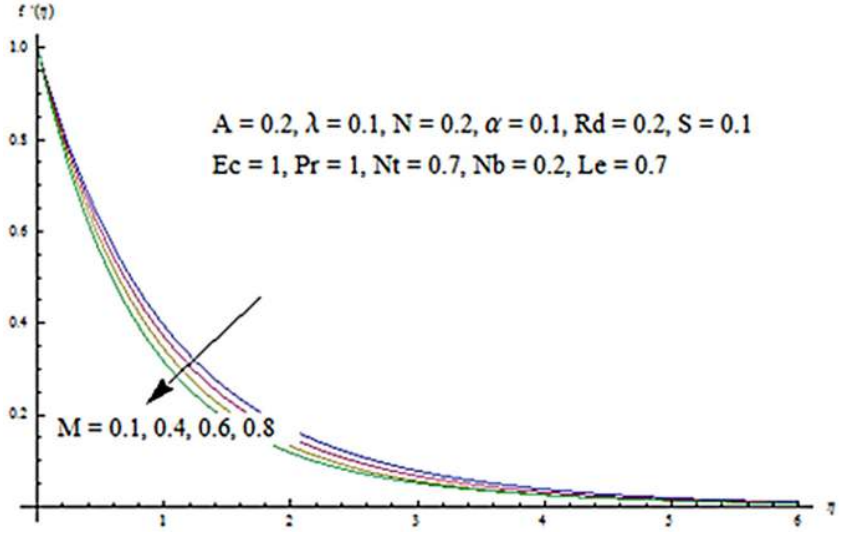

Fig 24. Influence of *M* on *f′*.

doi:10.1371/journal.pone.0124929.g024

Table 1. Convergence of series solutions for different order of approximations when $A = 0.2$, $M = 0.1$, $\lambda = 0.1$, $N = 0.2$, $\alpha = 0.1$, $Rd = 0.2$, $Ec = 1.0$, $Pr = 1.0$, $Nt = 0.7$, $Nb = 0.2$, $Le = 0.7$, $S = 0.1$ and for $\hbar = -0.7$.

Order of approximations	$-f''(0)$	$-\theta'(0)$	$-\phi'(0)$
1	0.99800	0.77022	0.39400
4	0.97740	0.78347	0.35521
6	0.97560	0.78815	0.40701
10	0.97500	0.78986	0.42402
13	0.97498	0.78993	0.42438
16	0.97498	0.78993	0.42413
25	0.97498	0.78993	0.42412

doi:10.1371/journal.pone.0124929.t001

Table 2. Numerical values of skin friction coefficient $C_f \mathrm{Re}_x^{1/2}$, local Nusselt number $Nu\mathrm{Re}_x^{-1/2}$ and sherwood number $Sh\mathrm{Re}_x^{-1/2}$ for different parameters when *Pr* = 1 = *Ec*, *Nt* = 0.7, *Nb* = 0.2, *Le* = 0.7 and *S* = 0.1.

A	*M*	*λ*	*N*	*α*	*Rd*	$-C_f\mathrm{Re}_z^{1/2}$	$-Nu\mathrm{Re}_z^{-1/2}$	$-Sh\mathrm{Re}_z^{-1/2}$
0.2	0.1	0.1	0.2	0.1	0.2	1.30339	0.65362	0.04239
0.1						1.25073	0.59409	0.06537
0.2						1.30339	0.65362	0.04239
0.3						1.35471	0.70814	0.03112
	0.2					1.32151	0.64652	0.02728
	0.3					1.35117	0.63492	0.03191
	0.4					1.39169	0.61901	0.03272
		0.1				1.30339	0.65362	0.04239
		0.2				1.21428	0.69074	0.11761
		0.3				1.12988	0.72281	0.18316
			0.1			1.31660	0.64633	0.02989
			0.2			1.30339	0.65362	0.04239
			0.3			1.29044	0.66062	0.05457
				0.1		1.30339	0.65362	0.04239
				0.2		1.53602	0.65094	0.01518
				0.3		1.74899	0.64792	0.01032
					0.1	1.30496	0.67833	0.09838
					0.2	1.30339	0.65362	0.04239
					0.3	1.30192	0.63123	0.00784

doi:10.1371/journal.pone.0124929.t002

Table 3. Numerical values of skin friction coefficient $C_f \mathrm{Re}_x^{1/2}$, local Nusselt number $Nu\mathrm{Re}_x^{-1/2}$ and sherwood number $Sh\mathrm{Re}_x^{-1/2}$ for different parameters when *A* = 0.2, *M* = 0.1, *λ* = 0.1, *α* = 0.1, *N* = 0.2 and *Rd* = 0.2.

Pr	*Nt*	*Nb*	*Le*	*S*	*Ec*	$-C_f\mathrm{Re}_z^{1/2}$	$-Nu\mathrm{Re}_z^{-1/2}$	$-Sh\mathrm{Re}_z^{-1/2}$
0.5						1.28232	0.51721	0.27114
0.8						1.28679	0.61215	0.15009
1.2						1.30856	0.68367	0.07743
	0.5					1.30846	0.67376	0.21774
	0.7					1.30339	0.65362	0.04239
	0.9					1.29856	0.63442	0.02745
	1.0					1.29621	0.62517	0.02612
		0.1				1.28926	0.68457	1.25400
		0.2				1.30339	0.65362	0.042416
		0.3				1.30783	0.62998	0.035137
			0.5			1.29825	0.66993	0.38878
			0.7			1.30339	0.65362	0.04239
			0.9			1.30687	0.64212	0.02374
				0.2		1.36652	0.66523	0.06457
				0.3		1.43250	0.67692	0.08701
				0.4		1.50128	0.68871	0.10960
					0.5	1.30572	0.78782	0.44115
					1.0	1.30339	0.65362	0.04239
					1.5	1.30107	0.51990	0.035497

doi:10.1371/journal.pone.0124929.t003

Table 4. Nomenclature.

Nomenclature			
B(t)	Magnetic field	T	Fluid temperature
(u, v)	Velocity components	T_∞	Ambient temperature
μ	Dynamic viscosity	C_∞	Ambient concentration
υ	Kinematic viscosity	βc	Concentration coefficient
ρ	Fluid Density	Pr	Prandtl number
α_1, α_2	Second grade parameters	Ec	Eckert number
σ^*	Stefan-Boltzmann constant	λ	mixedconvection parameter
Cp	Specific heat	q_r	radiative heat flux
κ	Thermal conductivity	Le	Lewis number
β_T	Thermal expansion coefficient	C_f	Skin friction
σ	Electrical conductivity	τ_w	Wall shear stress
q_w	Surface heat flux	j_w	Mass flux
A	Unsteady parameter	Nu_x	Nusselt number
g	Gravitational acceleration	q_w	Surface heat flux
G_{r_x}	Grashof number	R_d	radiation parameter
N_B	Brownian motion parameter	N_T	Thermophoresis parameter
D_B	Brownian diffusion coefficient	Re_x	Local Reynolds number
D_T	Thermophoretic diffusion coefficient	ψ	Stream function
κ^*	Mean absorption coefficient	η	Dimensionlessvariable
U_W	Stretching surface velocity	f	Dimensionless stream function
θ	Dimensionless temperature	ϕ	Dimensionless concentration
L_f	Linear operator for momentum	L_θ	Linear operator for energy
L_ϕ	Linear operator for concentration	$\hbar_\theta$	Auxiliary parameter for energy
$\hbar_f$	Auxiliary parameter for momentum	$\hbar_\phi$	Auxiliary parameter for concentration
S	Suction/injection parameter	a, c	Dimensional constants
T_w	Wall temperature	M	Hartman number
Sh	Sherwood number	V_w	Suction /injection velocity
t	time	C_w	Wall concentration

doi:10.1371/journal.pone.0124929.t004

- An increase in second grade parameter results in an increase in temperature and thermal boundary layer thickness but a decrease is seen for the nanoparticle concentration profiles
- Thermal boundary layer thickness and temperature $\theta(\eta)$ decrease by increasing buoyancy parameter λ.
- *Nt* and *Nb* are increasing functions of the temperature $\theta(\eta)$ whereas they depict an opposite behavior in case of Concentration ϕ.
- Pr decreases with an increase in values of temperature θ and concentration ϕ.
- For increasing values of λ, Skin friction coefficient and local Nusselt number increase whereas sherwood number decreases.
- *Le* show an opposite behavior for temperature θ and concentration ϕ.

Author Contributions

Analyzed the data: MR MB. Contributed reagents/materials/analysis tools: MR MB. Wrote the paper: MR MB.

References

1. Choi SUS. Enhancing thermal conductivity of fluids with nanoparticles, Proceeding of ASME Int.Mech. Eng.Congr.Expo, San Francisco, Calif, USA. 1995;66:99–105.
2. Azizian R, Doroodchi E, McKrell T, Buongiorno J, Hu LW, Moghtaderi B. Effect of Magnetic Field on Laminar Convective Heat Transfer of Magnetite Nanofluids. Int J Heat Mass Transfer. 2014; 68:94–109. doi: 10.1016/j.ijheatmasstransfer.2013.09.011
3. Rizvi IH, Jain A, Ghosh SKR, Mukherjee PS. Mathematical modelling of thermal conductivity for nano-fluid considering interfacial nano-layer. Heat Mass Transfer. 2013; 49:559–600. doi: 10.1007/s00231-013-1117-z
4. Alsaedi A, Awais M, Hayat T. Effects of heat generation/absorption on stagnation point flow of nanofluid over a surface with convective boundary conditions. Commun Nonlinear Sci Numer Simul. 2012; 17 (11):4210–4223. doi: 10.1016/j.cnsns.2012.03.008
5. Gümgüm S, Tezer Sezgin M. DRBEMsolution of mixed convection flow of nanofluids in enclosures with moving walls. J Comput Appl Math. 2014; 259(15):730–740.
6. Chamkha A, Gorla RSR, Ghodeswar K. Natural Convective Boundary Layer Flow Over a Vertical Cone Embedded in a Porous Medium Saturated with a Nanofluid. J Nanofluids. 2014; 3(1):65–71. doi: 10.1166/jon.2014.1074
7. Makinde OD, Khan WA, Khan ZH. Buoyancy effects on MHD stagnation point flow and heat transfer of a nanofluid past a convectively heated stretching/shrinking sheet. Int J Heat Mass Transf. 2013; 62:526–533. doi: 10.1016/j.ijheatmasstransfer.2013.03.049
8. Sheikholeslami M, Ganji DD. Heat transfer of Cu-water nanofluid flow between parallel plates. Powder Technol. 2013; 235:873–879. doi: 10.1016/j.powtec.2012.11.030
9. Mahian O, Kianifar A, Kalogirou SA, Pop I, Wongwises S. A review of the applications of the nanofluids in solar energy. Int J Heat Mass Transfer. 2013; 57:582–594. doi: 10.1016/j.ijheatmasstransfer.2012.10.037
10. El-Dawy HA, Mohammadein AA, Gorla RSR. Effect of Magnetic Field on Free Convection Boundary Layer Flow Over a Vertical Surface in a Porous Medium Saturated with a Nanofluid, J Nanofluids, 2014; 3(1):72–77. doi: 10.1166/jon.2014.1077
11. Hussain T, Shehzad SA, Hayat T, Alsaedi A, Solamy F, Ramzan M. Radiative Hydromagnetic Flow of Jeffrey Nanofluid by an Exponentially Stretching Sheet. PLoS ONE. 2014; 9(8)e103719. doi: 10.1371/journal.pone.0103719 PMID: 25084096
12. Makinde OD. On MHD heat and mass transfer over a moving vertical plate with a convective surface boundary condition. Can J Chem Eng. 2010; 88(6);983–990. doi: 10.1002/cjce.20369
13. Zheng L, Niu J, Zhang X, Gao Y. MHD flow and heat transfer over a porous shrinking surface with velocity slip and temperature jump. Mathe Comp Model. 2012; 56:133–144. doi: 10.1016/j.mcm.2011.11.080
14. Jamila M, Rauf A, Fetecau C, Khan NA. Helical flows of second grade fluid due to constantly accelerated shear stresses. Commun Nonlinear Sci Numer Simul. 2011; 16(4):1959–1969. doi: 10.1016/j.cnsns.2010.09.003
15. Hayat T, Shehzad SA, Qasim M, Obaidat S. Flow of a second grade fluid with convective boundary conditions, Therm Sci. 2011; 15(2):253–261.
16. Turkyilmazoglu M. Dual and triple solutions for MHD slip flow of non-Newtonian fluid over a shrinking surface. Comput Fluids. 2011; 70:53–58. doi: 10.1016/j.compfluid.2012.01.009
17. Ashorynejada HR, Javaherdehb K, Sheikholeslamic M, Ganjic DD. Investigation of the heat transfer of a non-Newtonian fluid flow in an axisymmetric channel with porous wall using Parameterized Perturbation Method (PPM), J Frank Inst. 2014; 351(2):701–712. doi: 10.1016/j.jfranklin.2013.04.027
18. Hayat T. Second grade fluid flow with Powe-Law heat flux and heat source. Heat Transf. Res. 2013; 44 (8):687–702. doi: 10.1615/HeatTransRes.2012005716
19. Hayat T, Hussain T, Shehzad SA, Alsaedi A. Thermal and Concentration Stratifications Effects in Radiative Flow of Jeffrey Fluid over a Stretching Sheet, PLoS ONE. 2014; 9(10):e107858. doi: 10.1371/journal.pone.0107858 PMID: 25275441
20. Hayat T, Farooq M, Alsaedi A, Iqbal Z. Melting heat transfer in the stagnation point flow of Powell-Eyring fluid, J Therm Heat Trans. 2013; 27:761–766. doi: 10.2514/1.T4059

21. Liao SJ. Beyond Perturbation. Boca. Raton: Chapman & Hall/CRC Press;2003.
22. Hayat T, Qasim M, Abbas Z. Homotopy solution for unsteady three dimensional MHD flow and mass transfer in a porous space, Commun Nonlinear Sci Numer Simul. 2010; 15:2375–2387. doi: 10.1016/j.cnsns.2009.09.013
23. Hayat T, Shehzad SA, Qasim M, Alsaedi A. Mixed convection flow by a porous sheet with variable thermal conductivity and convective boundary condition. Brazilian J Chem Eng. 2014; 31(1):109–117. doi: 10.1590/S0104-66322014000100011
24. Bataineh AS, Noorani MSM, Hashim I. Modified homotopy analysis method for solving system of second order BCVPs. Commun Nonlinear Sci Numer Simulat. 2009; 14:430–442. doi: 10.1016/j.cnsns.2007.09.012
25. Shehzad SA, Hayat T, Qasim M, Asghar S. Effects of mass transfer on MHD flow of casson fluid with chemical reaction and suction. Brazilian J Chem Eng. 2011; 30(1):187–195. doi: 10.1590/S0104-66322013000100020
26. Ramzan M, Farooq M, Alsaedi A, Hayat T. MHD three-dimensional flow of couple stress fluid with Newtonian heating. Euro Phy J Plus. 2013; 128:49–63. doi: 10.1140/epjp/i2013-13049-5